

# An Intention-Driven Lane Change Framework Considering Heterogeneous Dynamic Cooperation in Mixed-Traffic Environments

Xiaoyun Qiu, Haichao Liu, Yue Pan, Jun Ma, and Xinhu Zheng\*

**Abstract**—In mixed-traffic environments, where autonomous vehicles (AVs) must interact with diverse human-driven vehicles (HVs), the unpredictability of human intentions and heterogeneous driving behaviors poses significant challenges to safe and efficient lane change maneuvers. Existing methods often oversimplify these interactions by assuming uniform or fixed behavioral patterns. To address this limitation, we propose an *intention-driven lane change framework* that integrates driving-style recognition with cooperation-aware decision-making and motion-planning. First, a deep learning-based classifier is developed to identify distinct human driving styles from the NGSIM dataset in real time. Second, we introduce a cooperation score composed of intrinsic and interactive components, which estimates surrounding drivers’ intentions and quantifies their willingness to cooperate with the ego vehicle’s lane change. Third, a decision-making module is designed by combining behavior cloning (BC) with inverse reinforcement learning (IRL) to determine whether a lane change should be initiated under current conditions. Finally, a coordinated motion-planning architecture is established, integrating IRL-based intention inference with model predictive control (MPC) to generate collision-free and socially compliant trajectories. Extensive experiments demonstrate that the proposed intention-driven BC-IRL model achieves superior performance, reaching 94.2% accuracy and 94.3% F1-score, and outperforming multiple rule-based and learning-based baselines. In particular, it improves lane change recognition by 4–15% in F1-score, highlighting the benefit of modeling inter-driver heterogeneity via intrinsic and interactive cooperation scores. By bridging the gap between real-world human behaviors and automated lane change strategies, this work advances the development of context-aware and human-like AV systems for safe and efficient operations in complex traffic environments.

**Index Terms**—mixed-traffic environment, lane change decision-making, human driving style, inverse reinforcement learning, intention-driven interaction, NGSIM

## I. INTRODUCTION

The rapid advancement of autonomous driving technology has accelerated the transition toward mixed-traffic environments where autonomous vehicles (AVs) will inevitably share roadways with human-driven vehicles (HVs) for the foreseeable future [1]. Within this operational paradigm, the ability of AVs to accurately interpret and adapt to human

drivers’ heterogeneous behavioral patterns during lane change maneuvers emerges as a critical safety imperative [2], [3]. This challenge is particularly acute given the fundamental uncertainty inherent in human decision-making processes and the dynamic complexity of traffic interactions [4].

Modern lane change algorithms have evolved from classical models [5] to contemporary data-driven approaches [6], [7], and can be broadly categorized into three paradigms: rule-based, data-driven, and incentive-based systems. Recent advances in inverse reinforcement learning [8] and probabilistic modeling [9] have partially incorporated driver intentions into decision-making [10]. Nevertheless, several critical limitations persist. Firstly, existing frameworks often rely on a behavioral homogeneity assumption, which oversimplifies surrounding human drivers by adopting uniform behavioral models and thereby overlooks inter-driver heterogeneity in decision-making. Secondly, although some methods incorporate personalized intentions, they typically fail to capture the temporal evolution of interactions among surrounding vehicles. Lastly, there remains an intention modeling gap: current prediction approaches lack mechanisms to effectively link observable driving styles with latent reward structures, resulting in a disconnect between behavior recognition and motion-planning.

These limitations are particularly problematic given that sudden lane changes account for about 17.0% of total severe crashes [11], underscoring the urgent need for AV frameworks capable of simultaneously predicting trajectories and adapting to individual driving styles [12].

To address the identified shortcomings in existing algorithms, we introduce an intention-driven lane change framework that synergistically integrates driving-style recognition with adaptive decision-making as shown in Fig.1. In the context of this research, “driving style” is conceptualized as a habitual manner of vehicle operation, distinctive of an individual or subset of drivers, that serves as a proxy for underlying personalized driving intentions. Our proposed lane change framework incorporates driving style into two distinct yet interrelated components: intention-prediction and motion-planning. The main contributions of this study are summarized as follows:

- We introduce a cooperation score to quantify human drivers’ cooperative intentions during lane change interactions, where adaptive parameters are optimized to align with diverse driving styles.
- We design a dual-perspective intention-prediction framework that integrates intrinsic vehicle states with interac-

\*Corresponding author

X. Qiu, Y. Pan, J. Ma, and X. Zheng are with the Intelligent Transportation Thrust, Systems Hub, The Hong Kong University of Science and Technology (Guangzhou), Guangzhou, China, and with the Guangdong Provincial Key Lab of Integrated Communication, Sensing and Computation for Ubiquitous Internet of Things, Guangzhou, China.

H. Liu and J. Ma are with the Robotics and Autonomous Systems Thrust, Systems Hub, The Hong Kong University of Science and Technology (Guangzhou), Guangzhou, China.

tive contextual cues, thereby improving the interpretability, adaptability, and prediction accuracy of cooperation-aware lane change behavior.

- We develop a BC-IRL integrated decision-making model that produces human-like lane change strategies conditioned on the inferred cooperation score and surrounding traffic context.
- We propose an IRL-MPC pipeline that jointly learns driver-specific reward functions and generates collision-free, kinematically feasible trajectories, enabling safe and personalized maneuver planning.

## II. RELATED WORK

### A. Automated Lane Change Algorithms

Lane change algorithms have evolved from Gipps' seminal car-following model [5] into three methodological paradigms: rule-based, data-driven, and incentive-based approaches [6], [7]. These paradigms reflect the shift from handcrafted heuristics toward learning- and optimization-driven strategies, yet each exhibits inherent strengths and weaknesses.

**Rule-based methods** rely on predefined criteria to reproduce lane change behaviors. Representative studies include MOBIL [13], which minimizes overall braking induced by lane changes, and fuzzy-rule systems combined with LSTMs for maneuver forecasting [14]. Rule-based constraints have also been integrated into longitudinal control [15] and optimization formulations [16]. Although interpretable and computationally efficient, such approaches are rigid and sensitive to rule specification, often resulting in ambiguous decisions under complex traffic conditions.

**Data-driven methods** exploit large-scale trajectory datasets to learn nonlinear mappings between traffic states and lane change decisions. Classical examples include SVM-based classifiers [17] and ANN-SVM hybrids [18], while deep learning has enabled richer feature representation through DNNs [19]. Recent work further leverages Transformer architectures to capture temporal dependencies [20]. Despite improved accuracy, data-driven models often lack interpretability and generalizability, making their deployment in heterogeneous traffic environments non-trivial.

**Incentive-based methods** formulate lane change behavior as a sequential decision-making problem guided by rewards. Reinforcement learning has demonstrated promising results in adaptive driving policies [21], [22], but suffers from reward design difficulties and sparse exploration. Inverse reinforcement learning (IRL) alleviates this by recovering latent reward structures from demonstrations [8], [23], [24], enabling more human-like behavior synthesis. Nevertheless, IRL approaches remain computationally demanding and limited by state-space coverage.

In summary, rule-based methods offer interpretability but are limited by rigid assumptions, data-driven approaches achieve higher predictive accuracy but often lack interpretability and robustness, while incentive-based methods capture sequential decision-making but face challenges in reward design and scalability. Although both academic and industrial systems have demonstrated safe and efficient lane change performance

in constrained domains, existing frameworks still struggle to accommodate heterogeneous and dynamically evolving human behaviors. Motivated by these limitations, we leverage the complementary strengths of data-based learning (for accurate pattern recognition) and incentive-based reasoning (for human-like reward modeling) to design an intention-driven lane change framework that explicitly incorporates human drivers' cooperation intentions into the decision-making process.

### B. Lane Change Frameworks Considering Intention Prediction

To enhance safety and efficiency, recent lane change frameworks increasingly incorporate the prediction of surrounding HVs intentions. A number of studies have integrated intention prediction into decision-making pipelines [8]–[10].

Sun *et al.* [9] proposed a hierarchical decision-making model in which the first layer interacts with nearby vehicles to generate preliminary lane change decisions, while the second layer refines these into detailed trajectories. Guo *et al.* [25] improved adaptive cruise control by embedding merging-behavior prediction into car-following dynamics, thereby enhancing comfort and safety. Leveraging deep sequence models, Gao *et al.* [26] developed a dual-Transformer architecture that jointly predicts surrounding HVs' intentions and trajectories, demonstrating high accuracy by explicitly modeling social interactions. Zhao *et al.* [27] emphasized intention prediction within responsibility-sensitive safety frameworks, highlighting its role in proactive risk mitigation. More recently, Wang *et al.* [28] introduced a socially aware DAG-based intention-prediction algorithm, which further improves reliability by capturing structural dependencies among surrounding vehicles.

Despite these advances, most intention-aware frameworks still adopt simplifying assumptions. In particular, they often treat surrounding drivers as behaviorally homogeneous or rely on static personality traits, neglecting the dynamic interplay between driver heterogeneity and evolving traffic contexts. This limitation motivates approaches that explicitly integrate personalized and interactive cooperation intentions into lane change decision-making.

### C. Human Personality Integrated Lane Change Frameworks

In mixed-traffic environments, frameworks that integrate human personality factors offer more adaptive and realistic decision-making for AVs. Human factors have therefore been incorporated into both decision-making and motion-planning modules. Sheng *et al.* [10] designed a human-factor evaluation index emphasizing safety, efficiency, and comfort, which was subsequently embedded into a motion-planning algorithm that coordinated AV decisions with the interactive behaviors of surrounding vehicles. Liu *et al.* [29] incorporated benefit, safety, and tolerance factors into a support vector machine with Bayesian optimization to improve lane change rationality. Personalized driver traits have also been modeled explicitly: [30], [31], and [32] developed strategies that adapt lane change policies to driver-specific characteristics. Zhu *et al.* [33] proposed a personalized assistance system that prioritizes safety

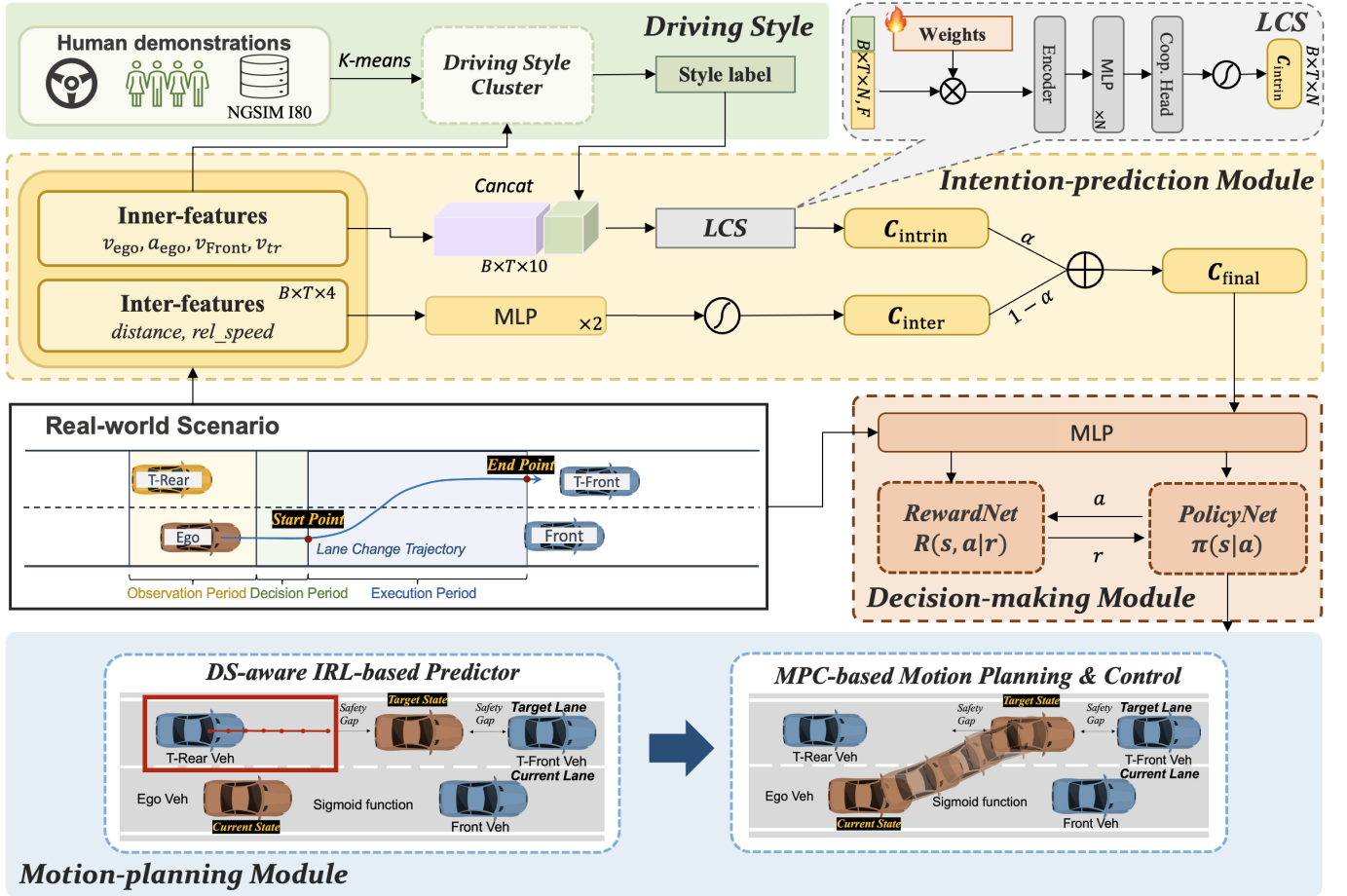


Fig. 1. Overall architecture of the proposed intention-driven lane change framework. (i) **Driving style recognition** provides discrete style labels; (ii) **Intention prediction** estimates cooperation levels via intrinsic learnable cooperation score (LCS) and interactive dynamic cooperation score (DCS), fused into  $c_{final}$ ; (iii) **Decision-making** integrates  $c_{final}$  with vehicle states to predict lane change intentions using policy and reward networks under a BC-IRL training objective; (iv) **Motion-planning** incorporates IRL-based trajectory prediction of surrounding vehicles and an MPC-based controller to generate safe, executable lane change trajectories.

by classifying drivers through a backpropagation neural network optimized with particle swarm methods. More recently, Liu *et al.* [34] introduced a human-like strategy that considers AV-HV interactions, thereby improving performance in mixed-traffic settings.

Despite these advances, existing research predominantly focuses on the host vehicle’s personality traits, while largely neglecting the intrinsic and interactive diverse intentions of surrounding human drivers. Yet these personalized cooperation intentions are critical for ensuring both safety and efficiency in lane change scenarios.

To address this gap, we propose an intention-driven lane change framework that explicitly models the dynamic cooperation willingness of surrounding drivers in the target lane. By embedding both intrinsic and interactive personality-informed intentions into decision-making, the framework aims to achieve safer and more socially compliant AV maneuvers.

### III. PROBLEM STATEMENT

To guarantee both the safety and efficiency of lane change maneuvers, it is essential to coordinate decisions based on the predicted personalized intentions of surrounding human

drivers. Accordingly, we propose an intention-driven lane change framework that includes the recognition of human driving styles and intention prediction, as illustrated in Fig. 1.

#### A. Problem Formulation

We consider a lane change scenario consisting of two adjacent lanes: the current lane occupied by the ego vehicle (AV, shown in red) and the target lane with surrounding human-driven vehicles (HVs, shown in blue and yellow). The ego vehicle’s decision is primarily influenced by two key HVs: the leading vehicle in the current lane and the target-rear (T-Rear) vehicle in the adjacent lane. Given the ego vehicle’s intention to merge, two candidate actions are defined: *lane change* (LC) and *lane keeping* (LK). Accordingly, the lane change decision-making problem is formulated as a binary classification task.

To mimic human driving processes, we model the environment as a Markov decision process (MDP) with state  $S$ , action  $A$ , and reward  $R$ . The **state space**  $S$  comprises both ego-vehicle states (velocity  $v_E$ , acceleration  $a_E$ ) and surrounding-vehicle observations, including the velocities of the leading and target-rear vehicles ( $v_f, v_{tr}$ ) and their relative distances

to the ego vehicle ( $d_{Ef}, d_{Etr}$ ). These features are grouped into *inner features* (ego-centric) and *inter features* (interaction-related). The **action space**  $A = \{LC, LK\}$  corresponds to either initiating a lane change or maintaining the current lane. The **reward**  $R$  represents the cumulative return defined by efficiency, safety, and comfort, and will be formally specified in Section IV.

The T-Rear vehicle plays a decisive role in determining whether the ego vehicle can safely execute a lane change. Its driving style, therefore, becomes a central factor in our framework, motivating the integration of human driver heterogeneity into both decision-making and motion-planning.

For clarity, the lane change process can be divided into three phases: 1) **Observation period**: the ego vehicle monitors surrounding states and infers the driving style of the T-Rear vehicle; 2) **Decision period**: the ego vehicle selects between LC and LK based on observed features and cooperation intention; 3) **Execution period**: once LC is chosen, the maneuver is carried out from initiation to completion.

## B. Dataset

This study employs the Next Generation SIMulation (NGSIM) I-80 dataset [35] for both training and evaluation. The dataset was collected on a section of the Interstate 80 freeway in California using multiple synchronized video cameras installed on nearby high-rise buildings. The recorded videos were subsequently processed to extract vehicle trajectories at a sampling rate of 10 Hz. The dataset provides detailed microscopic information such as vehicle position, velocity, and lane assignment, offering a naturalistic and high-resolution representation of mixed-traffic conditions. Owing to its comprehensiveness and accuracy, the NGSIM I-80 dataset has become one of the most widely adopted benchmarks for studying lane change behaviors and human-vehicle interactions.

To obtain reliable lane change episodes, we preprocess the raw dataset with the following filtering criteria:

- Only small passenger cars traveling within lanes 1–4 are retained.
- Each vehicle must exhibit exactly one lane change event within the monitored segment.
- The longitudinal span of the maneuver is constrained between 300 ft and 1,900 ft.
- A minimum duration of 10 seconds is preserved before and after the lane change event.
- Trajectories of the ego vehicle and its adjacent front and rear vehicles are extracted for both pre- and post-maneuver phases.

After filtering, a rolling median filter with a 5-s window and a Savitzky–Golay filter are sequentially applied to smooth the trajectories and reduce noise. Following these preprocessing steps, a total of 307 valid lane change episodes are extracted, each containing detailed trajectories of the ego vehicle and surrounding vehicles. Finally, to construct training samples, all trajectories are segmented into 2-s sliding windows, yielding a dataset of 5,295 samples in total: 3,666 LK samples and 1,629 LC samples.

---

## Algorithm 1: Lane Change Start-End Point Detection

---

**Input:** Lane change trajectory set  $X = \{x_1, x_2, \dots, x_n\}$   
**Output:** Start points  $t_s^1, t_s^2, \dots, t_s^n$ , End points  $t_e^1, t_e^2, \dots, t_e^n$

```

1 for  $k \leftarrow 1$  to  $n$  do
2    $v \leftarrow \text{diff}(x_k)$ 
3    $i_{\max} \leftarrow \arg \max_i |v_i|$ 
4   Initialize search parameters:  $i_{\text{left}} \leftarrow i_{\text{right}} \leftarrow i_{\max}$ ,
    $t_s \leftarrow t_e \leftarrow 0$ 
5    $\text{RMI} \leftarrow \{\}$ 
6    $\text{foundLaneChange} \leftarrow \text{False}$ 
7   while not  $\text{foundLaneChange}$  do
8      $i_{\text{left}} \leftarrow \text{SEARCHLANECHANGE}(v, i_{\max}, \delta, \text{left})$ 
9      $i_{\text{right}} \leftarrow \text{SEARCHLANECHANGE}(v, i_{\max}, \delta, \text{right})$ 
10    if  $\text{sgn}(v[i_{\max}]) = \text{sgn}(x_{k,\text{end}} - x_{k,\text{start}})$  and
    HASLANELINES( $x_k, i_{\text{left}}, i_{\text{right}}$ ) then
11       $\text{foundLaneChange} \leftarrow \text{True}$ 
12    else
13       $\text{RMI} \leftarrow \text{RMI} \cup \{i_{\max}\}$ 
14       $i_{\max} \leftarrow \arg \max_{i \notin \text{RMI}} |v_i|$ 
15   $t_s^k \leftarrow i_{\text{left}}$ 
16   $t_e^k \leftarrow i_{\text{right}}$ 

```

---



---

## Algorithm 2: Search Lane Change

---

**Input:** Lateral speed data  $v$ , lateral position data  $x$ , Start index  $t_{\text{start}}$ , Threshold  $\delta$ , Direction  $\text{dir}$ , Lane Width  $L$   
**Output:** Updated index  $t_{\text{LaneChange}}$ , Boolean  $\text{containsLaneLines}$

```

1  $t \leftarrow t_{\text{start}}$ 
2  $L_{\text{range}} \leftarrow \text{Arange}(0, \max(x) + L, L)$ 
3 while ( $\text{dir} = -1$  and  $t \geq 1$ ) or
   ( $\text{dir} = 1$  and  $t < \text{len}(v) - 1$ ) do
4    $\text{condition}_a \leftarrow |v[t]| \leq \delta$ 
5    $\text{condition}_b \leftarrow \text{sgn}(\Delta v, t) \neq \text{sgn}(\Delta v, t - 1)$ 
6    $l_s \leftarrow x[t]$ ,  $l_e \leftarrow x[t + \text{dir}]$ 
7    $\text{containsLaneLines} \leftarrow \text{any}(l_s \leq k \leq l_e \text{ or } l_s \geq k \geq$ 
    $l_e \text{ for } k \in L_{\text{range}})$ 
8   if  $\text{condition}_a$  and  $\text{condition}_b$  and
    $\text{containsLaneLines}$  then
9     return  $t$ ,  $\text{True}$ 
10   $t \leftarrow t + \text{dir}$ 
11 return 0 if  $\text{dir} = -1$  else  $\text{len}(v) - 1$ ,  $\text{False}$ 

```

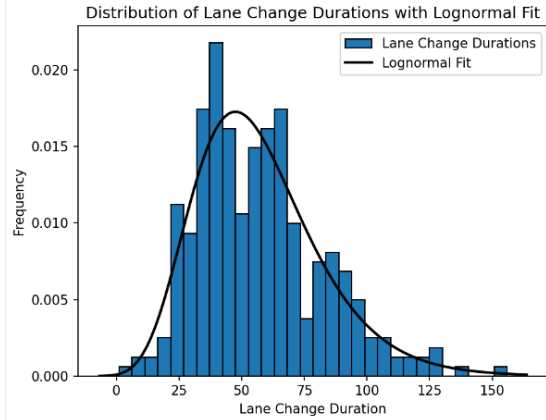
---

## C. Lane Change Start-End Point Detection

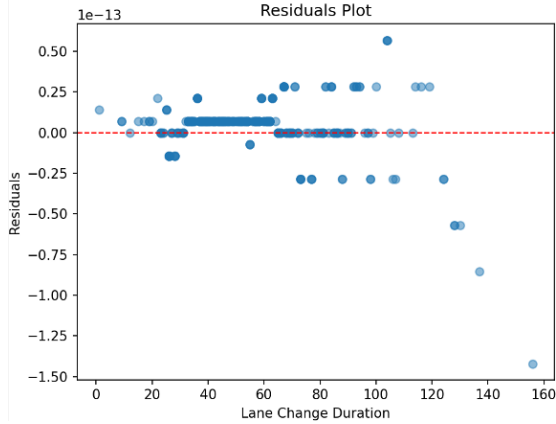
In this section, we introduce a novel approach for detecting the start and end points of lane changes, as delineated in Alg. 1. The detection process utilizes the vehicle’s lateral trajectory as input, with the lateral speed calculated to facilitate the identification of lane change points. Alg. 2 outlines the method for bidirectionally searching for lane change points, beginning at the timestep where the lateral speed peaks and continuing until it decreases to a specified lower threshold.

Additionally, we set forth a criterion to verify the continuous presence of lane lines, thereby reducing the likelihood of false detections. The efficacy of our detection algorithm is illustrated in Fig. 3, which highlights its capability to not only pinpoint rapid lane changes but also detect subtle lateral adjustments made by vehicles.

Upon identifying the start and end points, we compute the lane change duration. This methodology is applied to the lane



(a) Log-normal distribution of lane change duration.



(b) Residuals plot of the lane change duration.

Fig. 2. Analysis of lane change duration times. (a) The log-normal distribution fit of lane change duration times demonstrates the statistical behavior of lane changes. (b) The residuals plot helps identify any patterns of deviation from the model, indicating the accuracy and fit quality.

change trajectories extracted from our dataset, enabling the determination of their respective lane change durations. As shown in Fig. 2, the log-normal fit distribution of lane change duration times, along with its residuals plot, aligns closely with findings from previous research [36], [37], substantiating the precision of our algorithms in accurately identifying lane change start and end points.

#### IV. METHODOLOGY

This section presents our intention-driven decision-making and motion-planning framework for autonomous lane changes. The framework consists of four modules: (i) driving style clustering and recognition, (ii) intention prediction via cooperation scoring, (iii) decision-making with policy and reward networks, and (iv) motion-planning that generates executable trajectories. The overall workflow is shown in Fig. 1.

##### A. Driving Style Clustering and Recognition Module

To enable adaptive decision-making, the driving style of surrounding vehicles is recognized from their historical motion patterns. We adopt a two-stage procedure: (i) unsupervised clustering to establish representative driving styles, and (ii) supervised recognition for online classification.

TABLE I  
FEATURES SELECTED FOR DRIVING STYLE CLUSTERING

Symbol	Feature Description
$\bar{v}$	Average velocity
$\bar{a}$	Average acceleration
$v_{std}$	Std. deviation of velocity
$a_{std}$	Std. deviation of acceleration
$v_{max}$	Maximum velocity
$a_{max}$	Maximum acceleration

a) *Feature extraction and clustering*: From each vehicle trajectory, six statistical features are computed, including mean and maximum velocity/acceleration and their standard deviations (see Table I). To alleviate dimensionality issues, features are transformed via principal component analysis (PCA). K-means clustering is then applied to group drivers into three canonical styles (aggressive, normal, conservative), by minimizing the intra-cluster squared Euclidean distance. This unsupervised step provides discrete style labels without requiring manual annotation.

b) *Recognition model*: Once clustering labels are obtained, a supervised classifier is trained to predict the style of new trajectories in real time. The network takes the same six features as input and consists of two hidden layers (64 units each, ReLU activation), followed by a softmax output over three style categories. The trained recognizer  $f_{\text{style}}$  outputs probabilities  $p(\text{style}|s_t)$ , which are subsequently used in the intention-prediction module.

This procedure ensures that latent driving styles are consistently extracted from raw behavioral data and can be integrated into the cooperation-aware decision-making framework.

##### B. Intention-prediction Module

The intention-prediction module quantifies the cooperative tendency of surrounding drivers through two complementary scores: a *learnable intrinsic score* capturing style-conditioned cooperation and a *dynamic interactive score* derived from inter-vehicle interactions. These scores are subsequently fused through a trainable gating mechanism.

a) *Learnable Cooperation Score (LCS)*: The **intrinsic cooperation score** encodes cooperation tendencies specific to the target vehicle's internal driving style. It is computed by concatenating the inner features  $s_t$  with the style label, and projecting them through a learnable encoder  $f_{\text{intr}}$ :

$$c_t^{\text{intr}} = f_{\text{intr}}([s_t; \text{style}]; \theta_{\text{intr}}). \quad (1)$$

The parameters  $\theta_{\text{intr}}$  are trainable and receive gradients both from the cooperation regularization loss and from the downstream decision-making objective, ensuring that the learned score reflects intrinsic cooperation characteristics consistent with safe and efficient driving.

b) *Dynamic Cooperation Score (DCS)*: The **interactive cooperation score** reflects how a driver responds to its

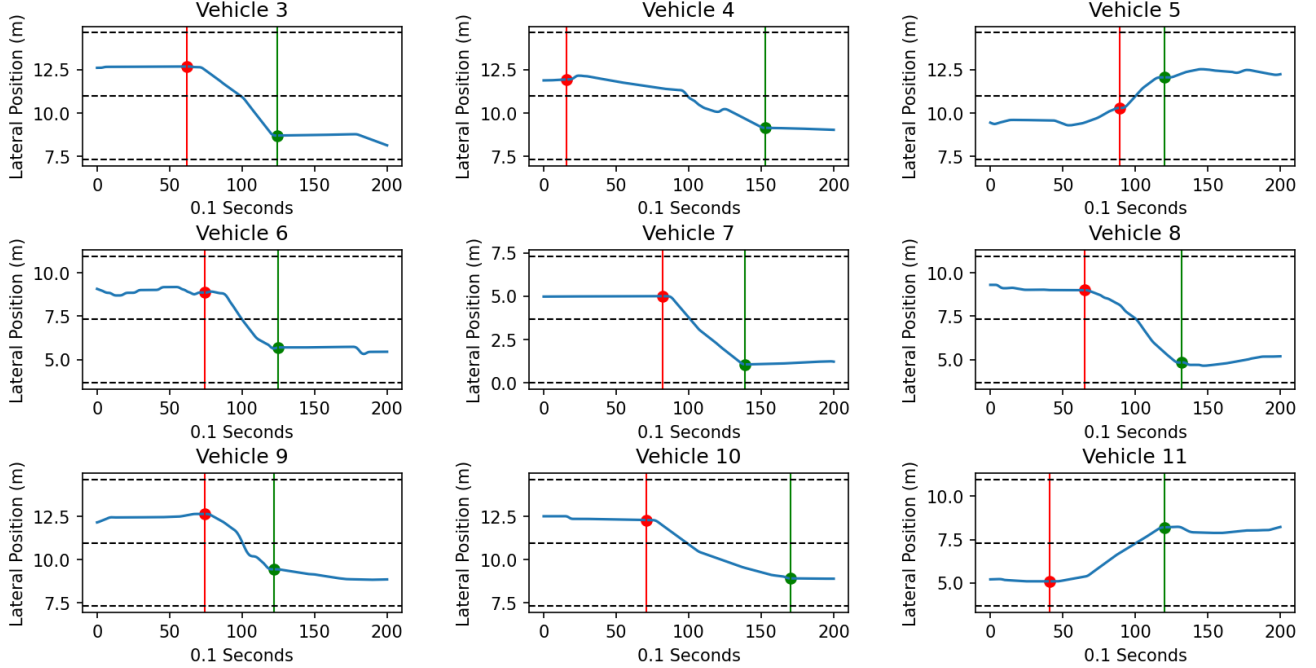


Fig. 3. Performance of the lane change start and end point detection algorithm. Spatial distribution of lane change points along vehicle trajectories is illustrated. Red dots denote the initiation points and green dots the termination points. The lane change duration, measured from the start to the end point, reflects the effectiveness and accuracy of the algorithm.

surrounding context, and is obtained from interaction-level features  $\mathbf{h}_t$  (e.g., relative distance, relative velocity):

$$c_t^{\text{inter}} = f_{\text{inter}}(\mathbf{h}_t; \theta_{\text{inter}}). \quad (2)$$

Unlike LCS, DCS adapts to momentary traffic interactions, complementing the long-term style-driven characterization.

The final cooperation score is produced through a learnable gate that dynamically balances the contributions of LCS and DCS:

$$c_t^{\text{final}} = \alpha_t \cdot c_t^{\text{intr}} + (1 - \alpha_t) \cdot c_t^{\text{inter}}, \quad (3)$$

with gating coefficient

$$\alpha_t = \sigma(\text{MLP}([\mathbf{s}_t, \mathbf{h}_t])). \quad (4)$$

The gate is fully differentiable and updated by gradient backpropagation, enabling context-dependent modulation of cooperation.

### C. Decision-making Module

The decision-making module integrates the fused cooperation score  $c_t^{\text{final}}$  with both inner and interaction features  $\{\mathbf{x}_t, \mathbf{h}_t\}$  to jointly learn a policy and a reward function. The whole algorithm can be found in Alg. 3

- **Policy Net**  $f_\pi$ : an LSTM-based classifier that outputs the probability  $\hat{a}_t$  of executing a lane change versus keeping lane, trained with a reward-weighted behavior cloning loss.
- **Reward Net**  $f_r$ : an auxiliary network optimized via inverse reinforcement learning, which estimates latent rewards  $r_t^{(a)}$  for each candidate action  $a$ . These rewards

are used both to shape the policy's weighted imitation and to enforce discriminability between cooperative and non-cooperative behaviors.

The overall training objective combines three components:

$$\mathcal{L} = \mathcal{L}_{\text{BC}} + \mathcal{L}_{\text{IRL}} + \mathcal{L}_{\text{coop}}, \quad (5)$$

where each term is defined as follows.

a) *Reward-weighted Behavior Cloning (BC) loss*: For each training instance  $(\mathbf{x}_i, \mathbf{h}_i, s_i, a_i)$ , the policy predicts a logit  $z_i = f_\pi(\mathbf{x}_i, \mathbf{h}_i, c_i^{\text{final}})$ . The per-sample BCE loss is

$$\ell_{\text{BCE}}^{(i)} = -[a_i \log \sigma(z_i) + (1 - a_i) \log(1 - \sigma(z_i))], \quad (6)$$

weighted by reward-based coefficients

$$w_i = \frac{\sigma(\beta(r_i^{(1)} - r_i^{(0)}))}{\frac{1}{B} \sum_{j=1}^B \sigma(\beta(r_j^{(1)} - r_j^{(0)}))}, \quad (7)$$

where  $r_i^{(1)}, r_i^{(0)}$  are reward estimates for LC and LK, respectively. The BC loss is then

$$\mathcal{L}_{\text{BC}} = \frac{1}{B} \sum_{i=1}^B w_i \ell_{\text{BCE}}^{(i)}. \quad (8)$$

This design exploits the stability of BC while injecting reward-driven preferences to emphasize more informative samples. Compared with pure IRL, which is prone to instability under limited demonstrations, reward-weighted BC offers a more robust training signal.

---

**Algorithm 3:** Training the Intention-driven Lane Change Decision-making Model
 

---

**Input:** Dataset  $\mathcal{D} = \{(\mathbf{x}, \mathbf{h}, s, a)\}$  with inner features  $\mathbf{x}$ , inter features  $\mathbf{h}$ , style label  $s$ , and binary label  $a$ . Hyperparameters: learning rate  $\eta$ , batch size  $B$ , epochs  $E$ , reward temperature  $\beta$ ,  $\lambda_2$  (L2 regularization),  $\lambda_s$  (margin).

**Output:** Trained  $f_{\text{intr}}$ ,  $f_{\text{inter}}$ ,  $f_\pi$ ,  $f_r$ .

```

1 Initialize  $f_{\text{intr}}$ ,  $f_{\text{inter}}$ ,  $f_\pi$ ,  $f_r$  and Adam optimizers with
  learning rate  $\eta$ .
2 for epoch  $\leftarrow 1$  to  $E$  do
3   foreach mini-batch  $\{(\mathbf{x}_i, \mathbf{h}_i, s_i, a_i)\}_{i=1}^B$  do
4     Compute LCS:  $c_i^{\text{intr}} \leftarrow f_{\text{intr}}([\mathbf{x}_i; s_i])$ ,
5     Compute DCS:  $c_i^{\text{inter}} \leftarrow f_{\text{inter}}(\mathbf{h}_i)$ ,
6      $\alpha_i \leftarrow \sigma(\text{MLP}([\mathbf{x}_i, \mathbf{h}_i]))$ ,
7      $c_i^{\text{final}} \leftarrow \alpha_i c_i^{\text{intr}} + (1 - \alpha_i) c_i^{\text{inter}}$ .
8     Predict decision:  $z_i \leftarrow f_\pi(\mathbf{x}_i, \mathbf{h}_i, c_i^{\text{final}})$ ,
9      $\ell_{\text{BCE}}^{(i)} \leftarrow -[a_i \log \sigma(z_i) + (1 - a_i) \log(1 - \sigma(z_i))]$ .
10    Predict rewards:  $r_i^{(1)} \leftarrow f_r(\mathbf{x}_i, \mathbf{h}_i, c_i^{\text{final}}, 1)$ ;
11     $r_i^{(0)} \leftarrow f_r(\mathbf{x}_i, \mathbf{h}_i, c_i^{\text{final}}, 0)$ ,
12     $w_i \leftarrow \frac{\sigma(\beta(r_i^{(1)} - r_i^{(0)}))}{\mathbb{E}[\sigma(\beta(r_i^{(1)} - r_i^{(0)}))]}$ .
13     $\mathcal{L}_{\text{BC}} \leftarrow \frac{1}{B} \sum_i w_i \ell_{\text{BCE}}^{(i)}$ .
14     $\mathcal{L}_{\text{IRL}} \leftarrow$ 
15     $-\frac{1}{B} \sum_i [r_i^{(a_i)} - \log(\exp(r_i^{(a_i)}) + \exp(r_i^{(1-a_i)}))]$ 
16     $+ \lambda_2 \frac{1}{B} \sum_i [(r_i^{(a_i)})^2 + (r_i^{(1-a_i)})^2]$ 
17     $+ \lambda_s \frac{1}{B} \sum_i |r_i^{(a_i)} - r_i^{(1-a_i)}|$ .
18     $\mathcal{L}_{\text{coop}} \leftarrow \frac{1}{B} \sum_i (c_i^{\text{final}} - 0.5)^2$ .
19     $\mathcal{L} \leftarrow \mathcal{L}_{\text{BC}} + \mathcal{L}_{\text{IRL}} + \mathcal{L}_{\text{coop}}$ .
20    Update  $\{\theta_{\text{intr}}, \theta_{\text{inter}}, \theta_\pi, \theta_r\}$  with Adam using  $\nabla \mathcal{L}$ .
21 return  $f_{\text{intr}}$ ,  $f_{\text{inter}}$ ,  $f_\pi$ ,  $f_r$ .
```

---

b) *Inverse Reinforcement Learning (IRL) loss:* For each instance, the reward net evaluates both the chosen action  $a_i$  and the alternative action  $1 - a_i$ :

$$r_i^{(a_i)} = f_r(\mathbf{x}_i, \mathbf{h}_i, c_i^{\text{final}}, a_i), \quad r_i^{(1-a_i)} = f_r(\mathbf{x}_i, \mathbf{h}_i, c_i^{\text{final}}, 1-a_i). \quad (9)$$

The IRL objective enforces preference consistency, with additional regularization:

$$\begin{aligned} \mathcal{L}_{\text{IRL}} = & -\frac{1}{B} \sum_{i=1}^B \left[ r_i^{(a_i)} - \log(\exp(r_i^{(a_i)}) + \exp(r_i^{(1-a_i)})) \right] \\ & + \lambda_2 \frac{1}{B} \sum_{i=1}^B \left[ (r_i^{(a_i)})^2 + (r_i^{(1-a_i)})^2 \right] \\ & + \lambda_s \frac{1}{B} \sum_{i=1}^B |r_i^{(a_i)} - r_i^{(1-a_i)}|. \end{aligned} \quad (10)$$

c) *Cooperation regularization loss:* To stabilize cooperation scores, we penalize deviations from the neutral value 0.5:

$$\mathcal{L}_{\text{coop}} = \frac{1}{B} \sum_{i=1}^B (c_i^{\text{final}} - 0.5)^2. \quad (11)$$

The joint loss  $\mathcal{L}$  is fully differentiable with respect to all parameters  $\{\theta_{\text{intr}}, \theta_{\text{inter}}, \theta_\pi, \theta_r\}$ , and optimization is performed end-to-end using Adam.

### D. Motion-planning Module

a) *IRL-based target vehicle trajectory prediction:* To predict the motion of surrounding vehicles, we adopt maximum-entropy inverse reinforcement learning (Max-Ent IRL) [38]. Unlike behavior cloning, which directly maps states to actions, IRL infers the latent reward function  $R(s, a)$  that best explains expert demonstrations. Under the Max-Ent principle, the probability of a trajectory  $\zeta$  is

$$p(\zeta | \omega) = \frac{1}{Z(\omega)} \exp\left(\sum_t r(s_t)\right) \approx \frac{\exp\left(\sum_t \omega^T \mathbf{f}_\zeta\right)}{\sum_{\zeta'} \exp\left(\sum_t \omega^T \mathbf{f}_{\zeta'}\right)}, \quad (12)$$

where  $\omega$  is the reward weight vector,  $Z(\omega) = \sum_{\zeta'} \exp(\sum_t r)$  is the partition function,  $r$  is the cumulative reward,  $\mathbf{f}_\zeta$  is the feature vector of  $\zeta$ , and  $\zeta'$  represents a candidate trajectory. Parameters in  $\omega$  are identified and learned by maximizing the log-likelihood of expert trajectories:

$$\max_{\omega} L(\omega) = \sum_{\zeta \in \mathcal{D}} \log p(\zeta | \omega). \quad (13)$$

b) *Reward function design:* Following established formulations [39], the reward function is modeled as a linear combination of interpretable driving features:

$$R(s, a) = \omega^T \Phi(s, a), \quad (14)$$

where the feature vector  $\Phi(s, a)$  encodes three fundamental aspects of human driving behavior: Efficiency, Safety, and Comfort.

The **Efficiency** feature,  $f_{\text{eff}}(t)$ , reflects the vehicle's velocity magnitude, defined as:

$$f_{\text{eff}}(t) = |v_{\text{ego}}(t)| \quad (15)$$

The **Safety** feature,  $f_{\text{safety}}(t)$ , is designed to penalize short headways, ensuring a safe following distance, formulated as:

$$f_{\text{safety}}(t) = \exp\left(-\frac{x_{lv}(t) - x_{ego}(t)}{v_{ego}(t) + \epsilon}\right), \quad (16)$$

where  $x_{lv}$  and  $x_{ego}$  denote the positions of the leading and ego vehicles, respectively, and  $\epsilon$  is a small constant introduced to prevent division by zero.

The **Comfort** feature,  $f_{\text{comfort}}(t)$ , discourages abrupt maneuvers by incorporating the jerk (the derivative of acceleration,  $\dot{a}_{ego}(t)$ ) into its definition:

$$f_{\text{comfort}}(t) = 1 - \exp(-|\dot{a}_{ego}(t)|), \quad (17)$$

where  $\dot{a}_{ego}(t)$  is the jerk of the ego vehicle at time  $t$ .

Thus, the reward is accumulated as

$$R(s, a) = \omega_{\text{eff}} f_{\text{eff}} + \omega_{\text{safety}} f_{\text{safety}} + \omega_{\text{comfort}} f_{\text{comfort}}, \quad (18)$$

where the weights  $\{\omega_{\text{eff}}, \omega_{\text{safety}}, \omega_{\text{comfort}}\}$  are learned via Max-Ent IRL to balance efficiency, safety, and comfort in human-like trajectory prediction.

c) *MPC-based motion-planning and control*: With the lane change command of the proposed decision-making model, the AV is able to generate a lane change path based on the predicted trajectory of the target vehicle. Then MPC is used to control the AV drive from the current lane to the target lane considering the constraint of collision avoidance with the surrounding vehicles. Given the lane change command and the predicted trajectory of the following vehicle in the target lane, we generate a smooth lane change trajectory based on the Sigmoid function. To sufficiently utilize the predicted trajectory of the target vehicle, we generate the reference path of the AV using the Sigmoid function inspired by [40]. With the input of the predicted trajectory of the target vehicle, and the current and target state of the ego vehicle, the expression of the sigmoid function-based trajectory is elaborated as follows. The sigmoid function-based trajectory incorporates the predicted trajectory of the target vehicle along with the current and target states of the ego vehicle. With the expected longitudinal distance  $d_{\text{long}}$ , lateral distance  $d_{\text{lat}}$  during the lane change process, and the value of a curvature-related variable  $\tau$ , the reference path is generated by:

$$\begin{aligned} \tilde{x}(x) &= \hat{x} - \frac{d_{\text{long}}}{2}, \\ y(\tilde{x}) &= \frac{d_{\text{lat}}}{1 + e^{-\tau(\tilde{x}+b)}} + y_0, \end{aligned} \quad (19)$$

where  $\tilde{x}(x)$  is an intermediate variable, given  $\hat{x} \in [0, d_{\text{long}}]$ . With  $x(\hat{x}) = \hat{x} + x_0$ , we can generate a reference path for the AV to follow during the lane change process.

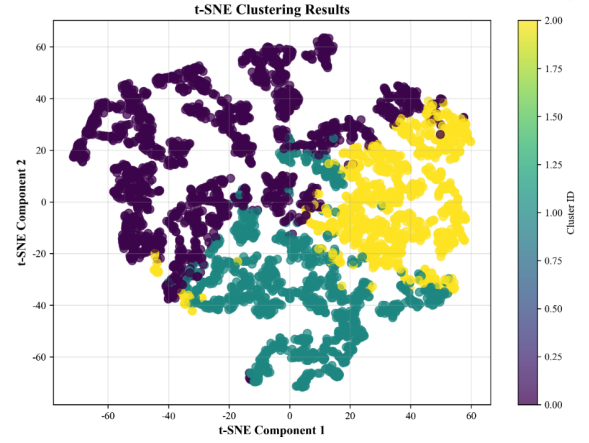
The expected lateral distance  $d_{\text{lat}}$  is predefined as the lane width, which is 3.6576 m by default. In contrast, the expected longitudinal distance is calculated by  $d_{\text{long}} = \bar{v}_{\text{T-Rear}} N \Delta T$ , where  $\bar{v}_{\text{T-Rear}}$  is the average velocity of the target vehicle based on the predicted trajectory using a specific method,  $N$  is the number of simulation steps,  $\Delta T = 0.1$  s is the simulation time interval. Concretely, the average velocity of the target vehicle can be calculated by differentiating its predicted positions generated by the trajectory prediction methods. Therefore, the trajectory prediction of the target vehicle is vital for the lane change behavior of the AV.

The generated reference trajectory is then integrated into the MPC controller for trajectory tracking and safety guarantee. We use a bicycle model to simulate the dynamics of the ego vehicle. Afterward, MPC is used to track the reference trajectory for lane change maneuvers. Next, following the recipe proposed in [41], each line of the road and the surrounding vehicles are modeled using potential functions integrated into the MPC-based trajectory.

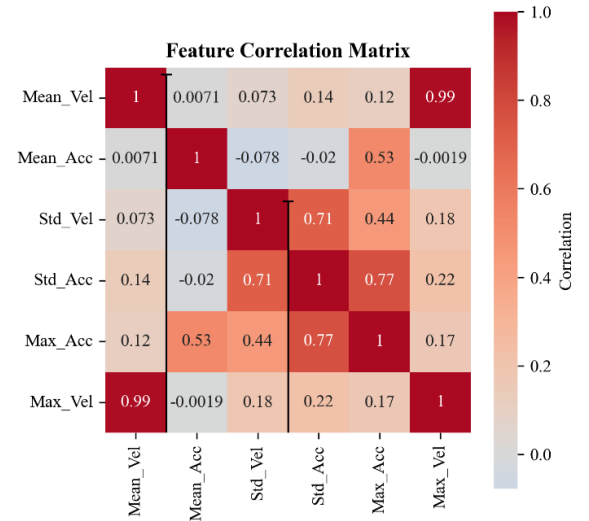
## V. EXPERIMENTS AND RESULTS

### A. Hyperparameter and Data Settings

The models were trained using the AdamW optimizer with a learning rate of  $1 \times 10^{-4}$  and a weight decay of  $1 \times 10^{-3}$ . The training was conducted for 200 epochs with a batch size of 128. For sequence modeling, the hidden dimension of the LSTM layers was set to 128. After preprocessing, a total of 5,295 samples were retained. The dataset was divided into



(a) Clustering results visualized using t-SNE.



(b) Feature correlation matrix of selected driving features.

Fig. 4. Analysis of driving-style representation: (a) clustering results show distinct style separation; (b) feature correlation matrix highlights inter-feature dependencies.

training and validation subsets with an 80/20 split, where stratified sampling was employed to maintain class balance between LK and LC. Each sample consisted of 10-dimensional state features (containing inner- and inter-features) over a sequence length of 20 frames.

### B. Main Results

The clustering results are shown in Fig. 4, the t-SNE manifest that the three groups are mostly separated well and the feature correlation matrix highlights inter-feature dependencies. To validate the impact of integrating human driving styles into the decision-making process, we compare the performance of our proposed model against baseline models:

- **IDM+MOBIL**: A rule-based baseline that integrates the Intelligent Driver Model (IDM) for longitudinal control [42] with the MOBIL framework for lateral maneuvers [13]. Lane change decisions are triggered by predefined safety constraints and acceleration incentives, aiming to balance efficiency and safety.

TABLE II  
COMPARISON OF DIFFERENT METHODS ON LANE KEEPING (LK) AND LANE CHANGE (LC) CLASSIFICATION.

Methods	overall metrics				LK			LC		
	accuracy	precision	recall	F1-score	precision	recall	F1-score	precision	recall	F1-score
IDM+MOBIL	0.6185	0.6394	0.6185	0.6269	0.7459	0.6808	0.7118	0.4000	0.4785	0.4358
H-LSTM	0.9112	0.9159	0.9112	0.9124	0.9584	0.9113	0.9343	0.8204	0.9110	0.8634
BC	0.8461	0.8502	0.8461	0.8477	0.9034	0.8728	0.8878	0.7275	0.7844	0.7549
VWC	0.9207	0.9219	0.9207	0.9211	0.9513	0.9332	0.9421	0.8559	0.8926	0.8739
<b>Ours</b>	<b>0.9418</b>	<b>0.9427</b>	<b>0.9418</b>	<b>0.9421</b>	<b>0.9656</b>	<b>0.9498</b>	<b>0.9576</b>	<b>0.8911</b>	<b>0.9239</b>	<b>0.9072</b>

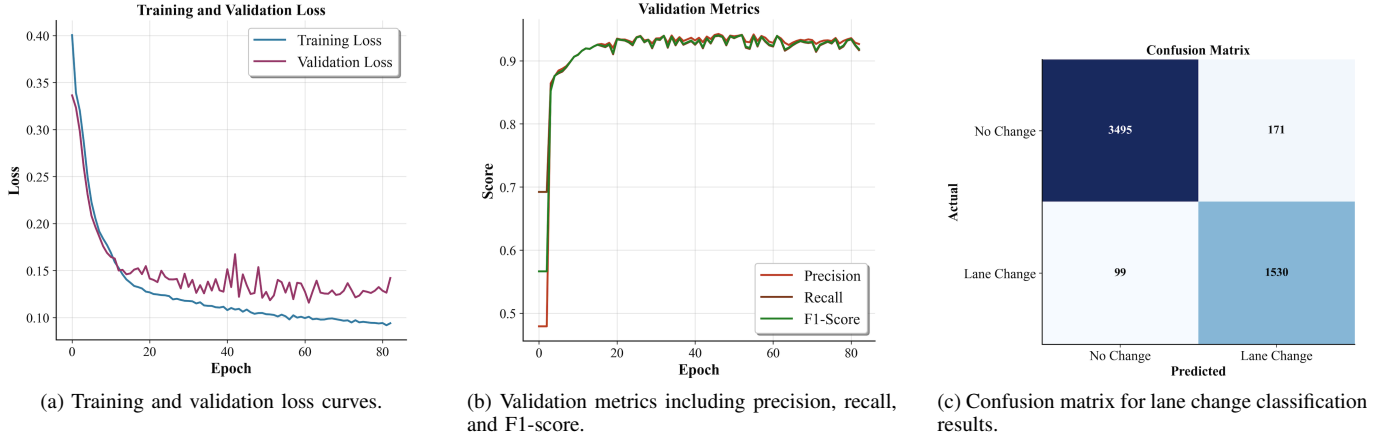


Fig. 5. Performance evaluation of the proposed intention-driven lane change decision-making model, including training dynamics, validation metrics, and classification outcomes.

- **H-LSTM**: A learning-based approach employing a hierarchical long short-term memory (H-LSTM) network [43] to capture temporal dependencies in multi-vehicle interactions and enable online lane change prediction.
- **BC**: A supervised imitation-learning baseline [44], where the policy directly maps state features to expert actions via behavior cloning, without explicit reward modeling.
- **VWC**: A learning-based baseline employing a variable-weight cooperation (VWC) model [45], which adaptively assigns dynamic weights to lane change conditions and driving demands across different phases of interaction.

Evaluation metrics for lane change intention prediction include precision, recall, and the F1 score, defined as follows [46]:

$$\text{precision} = \frac{TP}{TP + FP} \quad (20)$$

$$\text{recall} = \frac{TP}{TP + FN} \quad (21)$$

$$F1 = 2 \times \frac{\text{recall} \times \text{precision}}{\text{recall} + \text{precision}} \quad (22)$$

where  $TP$  denotes true positives, samples correctly predicted as  $LC$ ;  $FP$  denotes false positives,  $LK$  samples incorrectly predicted as  $LC$ ;  $FN$  denotes false negatives,  $LC$  samples incorrectly predicted as other decisions.

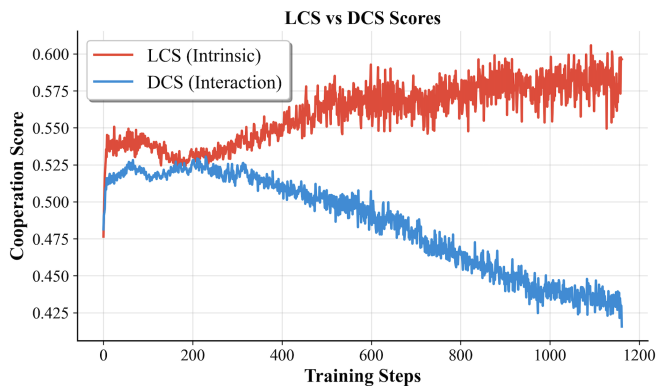
Table II compares the performance of different baselines against our proposed method on LK and LC classification. The results clearly show that rule-based IDM+MOBIL performs the worst, with overall accuracy of only 0.6185, reflecting its

limited adaptability to heterogeneous human driving patterns. Learning-based methods achieve significantly higher performance: H-LSTM reaches above 0.91 across all metrics by capturing temporal dependencies, while BC attains moderate performance (accuracy 0.8461) but is constrained by its reliance on direct imitation. The VWC model further improves classification accuracy to 0.9207 by adaptively weighting interactive features. In contrast, our proposed intention-driven BC-IRL framework achieves the best overall results, with accuracy 0.9418 and F1-score 0.9427. Notably, it improves lane change recognition (precision 0.8911, recall 0.9239, F1-score 0.9072) over all baselines, highlighting its ability to model inter-driver heterogeneity through cooperation scores and reward inference.

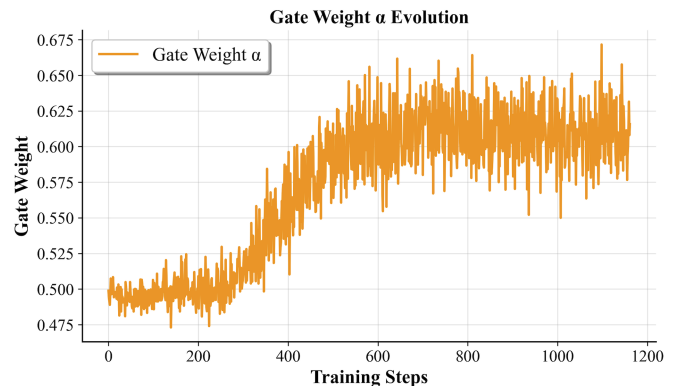
Fig. 5 further illustrates the training dynamics and classification outcomes. Fig. 5 (a) shows that both training and validation losses decrease steadily, with no significant overfitting, indicating stable convergence. Fig. 5 (b) reports the validation metrics (precision, recall, F1-score), all of which rapidly increase and stabilize around 0.9, demonstrating robust generalization. The confusion matrix in Fig. 5 (c) shows that the model achieves high true positive and true negative rates, with only a small number of misclassifications (171 false positives and 99 false negatives), confirming the effectiveness of the intention-driven decision-making framework in distinguishing LK and LC intentions.

TABLE III  
ABLATION STUDY RESULTS ON THE PROPOSED FRAMEWORK.

Core Module		Corp. Module		Metrics				
BC	IRL	LCS	DCS	Best F1	Accuracy	Precision	Recall	F1-score
✓				0.9383	0.9226	0.9306	0.9226	0.9240
✓	✓			0.9291	0.8905	0.9154	0.8905	0.8939
✓		✓		0.9438	0.9282	0.9357	0.9282	0.9296
✓	✓		✓	0.9408	0.9235	0.9305	0.9235	0.9249
✓	✓	✓	✓	<b>0.9531</b>	<b>0.9367</b>	<b>0.9437</b>	<b>0.9367</b>	<b>0.9379</b>



(a) Training performance of LCS (intrinsic cooperation score) and DCS (interactive cooperation score).



(b) Training performance of the gating weight  $\alpha_t$ .

Fig. 6. Convergence analysis of the cooperation-aware intention module: (a) intrinsic and interactive cooperation scores (LCS/DCS); (b) gating weight evolution during training.

### C. Ablation Study

Table III presents the ablation results of the proposed framework by selectively removing different core and cooperation modules. Using only the BC module achieves an F1-score of 0.9240, which indicates that pure behavior cloning provides a reasonable baseline but lacks robustness. Adding IRL alone degrades performance (F1-score 0.8939), suggesting that reward inference without supervised guidance may be unstable. Incorporating either the intrinsic cooperation score (LCS) or the dynamic cooperation score (DCS) individually improves the results (F1-scores 0.9296 and 0.9249, respectively), highlighting their complementary roles in modeling driver heterogeneity. The full model, which integrates BC, IRL, LCS, and DCS, achieves the best performance across all metrics, with an accuracy of 0.9367 and an F1-score of 0.9379. These findings demonstrate that BC and IRL are synergistic, where BC stabilizes learning while IRL enhances reward-driven generalization, and cooperation-aware modules (LCS and DCS) provide additional discriminative power by explicitly capturing intrinsic driver styles and interactive dynamics.

### D. Convergence Analysis of Cooperation-Aware Intention Module

Fig. 6 illustrates the training dynamics of the proposed cooperation-aware intention module. Fig. 6(a) reports the trajectories of the intrinsic learnable cooperation score (LCS) and the interactive dynamic cooperation score (DCS), while

Fig. 6(b) presents the evolution of the gating weight  $\alpha_t$  that adaptively balances these two components.

The results highlight three key observations. First, the LCS steadily increases throughout training and converges around 0.60, indicating that the model increasingly relies on intrinsic driver style features to capture cooperative intentions. In contrast, the DCS gradually decreases and stabilizes around 0.43, reflecting its role as a complementary but noisier signal derived from inter-vehicle interactions. This divergence suggests a natural division of labor, where LCS provides stable, style-dependent intention cues and DCS contributes local interaction corrections.

Second, the gating weight  $\alpha_t$  rises from approximately 0.45 to above 0.63, demonstrating that the model adaptively emphasizes LCS over DCS as training progresses. This self-adjusting weighting mechanism validates the necessity of the gating design, allowing the network to automatically balance intrinsic and interaction-based signals without manual tuning.

Finally, although the overall LCS converges to a consistent range, its distribution across samples still encodes the heterogeneity of driver behaviors. In other words, the learned cooperation scores retain sensitivity to diverse driving styles, while the gating mechanism ensures that interaction cues are not ignored but integrated proportionally. Collectively, these findings confirm the effectiveness of the dual-perspective intention modeling framework and the stability of its convergence behavior.

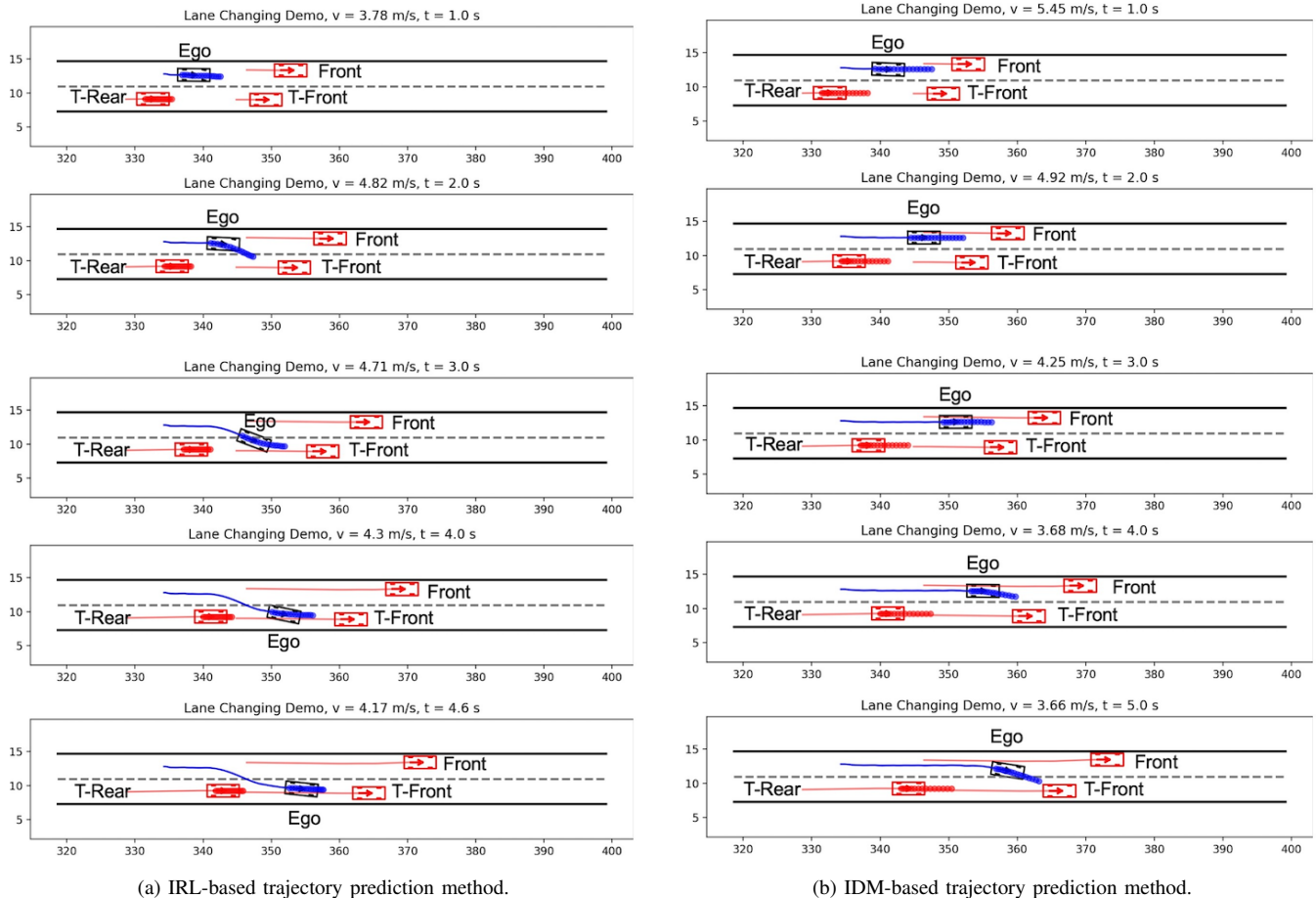


Fig. 7. Qualitative results. Comparison of MPC-based lane change performance with predicted trajectories of the T-Rear vehicle. The black vehicle represents the AV controlled by our driving framework. The three red vehicles symbolize the surrounding vehicles extracted from the NGSIM I-80 dataset. Blue bubbles indicate the trajectory generated by the MPC, and the red bubbles denote the predicted trajectory of the T-Rear vehicle.

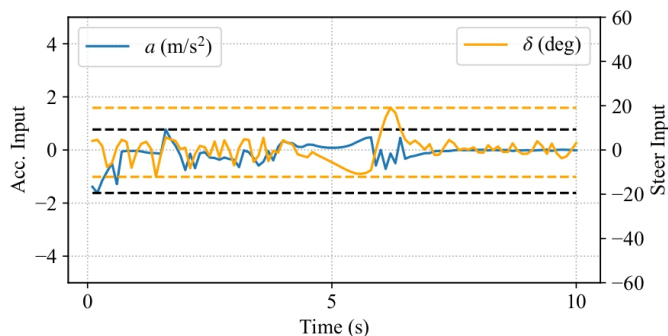


Fig. 8. The control input for the ego vehicle when executing lane change maneuver.

### E. Case Study

To qualitatively validate the motion-planning component, we analyze a representative lane change scenario and compare the proposed IRL-MPC approach with a traditional IDM baseline. Once a “LC” decision is made, the ego vehicle executes the maneuver while surrounding vehicles follow ground-truth trajectories from the NGSIM dataset. For comparison, the baseline ego vehicle behavior is generated by IDM, a widely used rule-based model in AV implementations.

Fig. 7 shows prediction snapshots at one-second intervals (10 steps) for the T-Rear vehicle. The left column illustrates our IRL-based method, while the right column shows IDM predictions. The results demonstrate that our method enables the ego vehicle to complete the lane change substantially faster and more efficiently. Specifically, in Fig. 7(a), the maneuver is completed within 4.6 seconds, whereas in Fig. 7(b), IDM requires 7.8 seconds and only reaches mid-transition at 4.6 seconds.

Beyond efficiency, the trajectories highlight differences in safety and adaptability. Under our approach, the ego vehicle initiates the lane change smoothly at a lower speed, maintaining a safe distance from the leading vehicle, and subsequently accelerates to finish the maneuver. In contrast, the IDM trajectory shows a delayed and slower transition, with higher potential safety risks due to less adaptive interaction with surrounding vehicles. These observations confirm that integrating reward-driven prediction and adaptive control yields lane changes that are not only more efficient but also safer and more human-like.

## VI. DISCUSSIONS AND CONCLUSION

### A. Limitations and Future Work

Despite the encouraging results, several limitations remain to be addressed in future work. First, while the current framework predicts the target vehicle's trajectory and cooperation intention, it does not explicitly account for alternative maneuvers such as yielding, accelerating, or defensive lane changes, which may critically influence the ego vehicle's planning. Second, our driving-style representation is restricted to three discrete categories, which simplifies heterogeneous human behaviors but overlooks finer-grained variations across drivers. Third, the current evaluation focuses on lane change scenarios, whereas real-world driving requires a broader spectrum of decisions, including car-following, merging, and gap acceptance in highly interactive contexts.

Future research will therefore extend cooperation modeling by incorporating multi-intention inference for surrounding vehicles, allowing the ego vehicle to better anticipate reactive behaviors. We also plan to enrich the driving-style taxonomy by leveraging unsupervised or semi-supervised clustering to capture more nuanced behavioral patterns. Finally, we aim to develop a multi-agent cooperative decision-making framework that integrates both vehicle-vehicle and vehicle-infrastructure interactions, enabling AVs to operate safely and efficiently in diverse and congested traffic environments.

### B. Conclusion

This paper presented an intention-driven lane change framework designed for mixed-traffic environments, where autonomous vehicles must adapt to heterogeneous and unpredictable human driving behaviors. The framework synergistically integrates driving-style recognition, cooperation-aware intention modeling, decision-making, and motion-planning. Specifically, a driving-style classifier was built on the NGSIM dataset to enable real-time recognition of aggressive, normal, and conservative drivers. On this basis, we introduced intrinsic and interactive cooperation scores to quantify surrounding drivers' cooperative intentions under different contexts. These scores were then incorporated into a BC-IRL decision-making model that balances supervised imitation with reward-driven generalization to determine when lane changes should be initiated. Finally, an IRL-MPC motion-planning module was employed to generate collision-free, socially compliant trajectories.

Experimental evaluations demonstrate that the proposed framework achieves superior performance, with 94.2% accuracy and 94.3% F1-score, consistently outperforming rule-based and learning-based baselines. Notably, it improves lane change recognition by 4–15% in F1-score, validating the effectiveness of explicitly modeling inter-driver heterogeneity. Beyond efficiency, the results also highlight improvements in safety and adaptability, confirming that cooperation-aware intention modeling facilitates more human-like decision-making and execution.

By bridging the gap between real-world human behaviors and automated decision-making, this study advances the development of context-aware autonomous driving systems.

Incorporating driving-style recognition, cooperation modeling, and reward-guided planning enables AVs to interact more naturally with human drivers, ultimately enhancing both safety and efficiency in complex traffic environments.

## REFERENCES

- [1] E. Yurtsever, J. Lambert, A. Carballo, and K. Takeda, "A survey of autonomous driving: Common practices and emerging technologies," *IEEE Access*, vol. 8, pp. 58 443–58 469, 2020.
- [2] Y. Xing, C. Lv, D. Cao, and P. Hang, "Toward human-vehicle collaboration: Review and perspectives on human-centered collaborative automated driving," *Transportation Research Part C: Emerging Technologies*, vol. 128, p. 103199, 2021.
- [3] L. Chen, Y. Li, C. Huang, B. Li, Y. Xing, D. Tian, L. Li, Z. Hu, X. Na, Z. Li *et al.*, "Milestones in autonomous driving and intelligent vehicles: Survey of surveys," *IEEE Transactions on Intelligent Vehicles*, vol. 8, no. 2, pp. 1046–1056, 2022.
- [4] W. Schwarting, J. Alonso-Mora, and D. Rus, "Planning and decision-making for autonomous vehicles," *Annual Review of Control, Robotics, and Autonomous Systems*, vol. 1, pp. 187–210, 2018.
- [5] P. G. Gipps, "A model for the structure of lane-changing decisions," *Transportation Research Part B: Methodological*, vol. 20, no. 5, pp. 403–414, 1986.
- [6] Z. Zheng, "Recent developments and research needs in modeling lane changing," *Transportation Research Part B: Methodological*, vol. 60, pp. 16–32, 2014.
- [7] Z. Wang, X. Shi, and X. Li, "Review of lane-changing maneuvers of connected and automated vehicles: models, algorithms and traffic impact analyses," *Journal of the Indian Institute of Science*, vol. 99, pp. 589–599, 2019.
- [8] Y. Sun, Y. Chu, T. Xu, J. Li, and X. Ji, "Inverse reinforcement learning based: Segmented lane-change trajectory planning with consideration of interactive driving intention," *IEEE Transactions on Vehicular Technology*, vol. 71, no. 11, pp. 11 395–11 407, 2022.
- [9] L. Sun, W. Zhan, and M. Tomizuka, "Probabilistic prediction of interactive driving behavior via hierarchical inverse reinforcement learning," in *2018 21st International Conference on Intelligent Transportation Systems (ITSC)*. IEEE, 2018, pp. 2111–2117.
- [10] Z. Sheng, L. Liu, S. Xue, D. Zhao, M. Jiang, and D. Li, "A cooperation-aware lane change method for automated vehicles," *IEEE Transactions on Intelligent Transportation Systems*, 2022.
- [11] M. Shawky, "Factors affecting lane change crashes," *IATSS research*, vol. 44, no. 2, pp. 155–161, 2020.
- [12] M. Kuderer, S. Gulati, and W. Burgard, "Learning driving styles for autonomous vehicles from demonstration," in *2015 IEEE International Conference on Robotics and Automation (ICRA)*, 2015, pp. 2641–2646.
- [13] A. Kesting, M. Treiber, and D. Helbing, "General lane-changing model mobil for car-following models," *Transportation Research Record*, vol. 1999, no. 1, pp. 86–94, 2007.
- [14] W. Wang, T. Qie, C. Yang, W. Liu, C. Xiang, and K. Huang, "An intelligent lane-changing behavior prediction and decision-making strategy for an autonomous vehicle," *IEEE Transactions on Industrial Electronics*, vol. 69, no. 3, pp. 2927–2937, 2021.
- [15] J. Wang, Q. Zhang, D. Zhao, and Y. Chen, "Lane change decision-making through deep reinforcement learning with rule-based constraints," in *2019 International Joint Conference on Neural Networks (IJCNN)*. IEEE, 2019, pp. 1–6.
- [16] S. He, J. Zeng, B. Zhang, and K. Sreenath, "Rule-based safety-critical control design using control barrier functions with application to autonomous lane change," in *2021 American Control Conference (ACC)*. IEEE, 2021, pp. 178–185.
- [17] H. M. Mandalia and M. D. D. Salvucci, "Using support vector machines for lane-change detection," in *Proceedings of the Human Factors and Ergonomics Society Annual Meeting*, vol. 49, no. 22. SAGE Publications Sage CA: Los Angeles, CA, 2005, pp. 1965–1969.
- [18] Y. Dou, F. Yan, and D. Feng, "Lane changing prediction at highway lane drops using support vector machine and artificial neural network classifiers," in *2016 IEEE International Conference on Advanced Intelligent Mechatronics (AIM)*. IEEE, 2016, pp. 901–906.
- [19] X. Liu, J. Liang, and B. Xu, "A deep learning method for lane changing situation assessment and decision making," *IEEE Access*, vol. 7, pp. 133 749–133 759, 2019.

- [20] X. Guo, H. Jia, Q. Huang, Q. Luo, N. Wang, and Z. Mao, "A vehicle driving intention prediction method based on gated dual tower transformer model for autonomous driving," *Expert Systems with Applications*, p. 128000, 2025.
- [21] C.-J. Hoel, K. Driggs-Campbell, K. Wolff, L. Laine, and M. J. Kochenderfer, "Combining planning and deep reinforcement learning in tactical decision making for autonomous driving," *IEEE Transactions on Intelligent Vehicles*, vol. 5, no. 2, pp. 294–305, 2019.
- [22] M. Zhu, X. Wang, and Y. Wang, "Human-like autonomous car-following model with deep reinforcement learning," *Transportation Research Part C: Emerging Technologies*, vol. 97, pp. 348–368, 2018.
- [23] S. Arora and P. Doshi, "A survey of inverse reinforcement learning: Challenges, methods and progress," *Artificial Intelligence*, vol. 297, p. 103500, 2021.
- [24] Z. Huang, J. Wu, and C. Lv, "Driving behavior modeling using naturalistic human driving data with inverse reinforcement learning," *IEEE Transactions on Intelligent Transportation Systems*, vol. 23, no. 8, pp. 10 239–10 251, 2021.
- [25] Y. Guo, Q. Sun, R. Fu, and C. Wang, "Improved car-following strategy based on merging behavior prediction of adjacent vehicle from naturalistic driving data," *IEEE Access*, vol. 7, pp. 44 258–44 268, 2019.
- [26] K. Gao, X. Li, B. Chen, L. Hu, J. Liu, R. Du, and Y. Li, "Dual transformer based prediction for lane change intentions and trajectories in mixed traffic environment," *IEEE Transactions on Intelligent Transportation Systems*, 2023.
- [27] N. Zhao, B. Wang, K. Zhang, Y. Lu, R. Luo, and R. Su, "Lc-rss: A lane-change responsibility-sensitive safety framework based on data-driven lane-change prediction," *IEEE Transactions on Intelligent Vehicles*, 2023.
- [28] J. Wang, Y. Jin, H. Taghavifar, F. Ding, and C. Wei, "Socially-aware autonomous driving: Inferring yielding intentions for safer interactions," *arXiv preprint arXiv:2504.20004*, 2025.
- [29] Y. Liu, X. Wang, L. Li, S. Cheng, and Z. Chen, "A novel lane change decision-making model of autonomous vehicle based on support vector machine," *IEEE Access*, vol. 7, pp. 26 543–26 550, 2019.
- [30] V. A. Butakov and P. Ioannou, "Personalized driver/vehicle lane change models for adas," *IEEE Transactions on Vehicular Technology*, vol. 64, no. 10, pp. 4422–4431, 2014.
- [31] J. Liu, L. N. Boyle, and A. G. Banerjee, "An inverse reinforcement learning approach for customizing automated lane change systems," *IEEE Transactions on Vehicular Technology*, vol. 71, no. 9, pp. 9261–9271, 2022.
- [32] S. Rosbach, V. James, S. Großjohann, S. Homoceanu, and S. Roth, "Driving with style: Inverse reinforcement learning in general-purpose planning for automated driving," in *2019 IEEE/RSJ International Conference on Intelligent Robots and Systems (IROS)*. IEEE, 2019, pp. 2658–2665.
- [33] B. Zhu, S. Yan, J. Zhao, and W. Deng, "Personalized lane-change assistance system with driver behavior identification," *IEEE Transactions on Vehicular Technology*, vol. 67, no. 11, pp. 10 293–10 306, 2018.
- [34] Y. Liu and S. Peeta, "Human-like lane-change control strategy for connected and autonomous vehicles to improve interactions with human-driven vehicles," *Transportation Research Part C: Emerging Technologies*, vol. 177, p. 105211, 2025.
- [35] J. Halkia and J. Colyar, "Interstate 80 freeway dataset," *Federal Highway Administration, US Department of Transportation*, 2006.
- [36] G. Li, Z. Yang, Y. Pan, and J. Ma, "Analysing and modelling of discretionary lane change duration considering driver heterogeneity," *Transportmetrica B: Transport Dynamics*, vol. 11, no. 1, pp. 343–360, 2023.
- [37] T. Toledo and D. Zohar, "Modeling duration of lane changes," *Transportation Research Record*, vol. 1999, no. 1, pp. 71–78, 2007.
- [38] B. D. Ziebart, A. L. Maas, J. A. Bagnell, A. K. Dey *et al.*, "Maximum entropy inverse reinforcement learning," in *AAAI*, vol. 8. Chicago, IL, USA, 2008, pp. 1433–1438.
- [39] X. Qiu, Y. Pan, M. Zhu, L. Yang, and X. Zheng, "Driving style-aware car-following considering cut-in tendencies of adjacent vehicles with inverse reinforcement learning," in *2024 IEEE Intelligent Vehicles Symposium (IV)*. IEEE, 2024, pp. 1329–1336.
- [40] M. Ammour, R. Orjuela, and M. Basset, "Trajectory reference generation and guidance control for autonomous vehicle lane change maneuver," in *2020 28th Mediterranean Conference on Control and Automation (MED)*. IEEE, 2020, pp. 13–18.
- [41] H. Liu, K. Chen, Y. Li, Z. Huang, M. Liu, and J. Ma, "UDMC: Unified decision-making and control framework for urban autonomous driving with motion prediction of traffic participants," *IEEE Transactions on Intelligent Transportation Systems*, vol. 26, no. 5, pp. 1–16, 2025.
- [42] A. Kesting, M. Treiber, and D. Helbing, "Enhanced intelligent driver model to access the impact of driving strategies on traffic capacity," *Philosophical Transactions of the Royal Society A: Mathematical, Physical and Engineering Sciences*, vol. 368, no. 1928, pp. 4585–4605, 2010.
- [43] X. Liao, Z. Wang, X. Zhao, Z. Zhao, K. Han, P. Tiwari, M. J. Barth, and G. Wu, "Online prediction of lane change with a hierarchical learning-based approach," in *2022 International Conference on Robotics and Automation (ICRA)*. IEEE, 2022, pp. 948–954.
- [44] L. Wang, C. Fernandez, and C. Stiller, "High-level decision making for automated highway driving via behavior cloning," *IEEE Transactions on Intelligent Vehicles*, vol. 8, no. 1, 2023.
- [45] X. Wang, Y. Zan, J. Zheng, Y. Tao, Y. Xiao, T. Li *et al.*, "Variable weight combination model for lane-changing prediction of human-driven vehicle," *IEEE Transactions on Intelligent Vehicles*, 2024.
- [46] D. Frossard, E. Kee, and R. Urtasun, "Deepsignals: Predicting intent of drivers through visual signals," in *2019 International Conference on Robotics and Automation (ICRA)*. IEEE, 2019, pp. 9697–9703.